Goethe-Universität Frankfurt am Main
Fachbereich 13: Physik
Institut für theoretische Physik

Bachelor Thesis

Methods of tree-level improvement of the static potential in SU(2) lattice Yang-Mills theory

---

Sonja Köhler

Frankfurt am Main
04.07.2022

First examiner and supervisor: Prof. Dr. Marc Wagner
Second examiner: Prof. Dr. Owe Philipsen

Abstract

The focus of this thesis is the reduction of discretization errors in lattice gauge theory computations of the static quark-antiquark potential. Specifically, two well-known and frequently used methods of tree-level improvement of the static potential are discussed and compared in detail using lattice simulations in the framework of SU(2) Yang-Mills theory.
Criteria for the effective reduction of discretization errors assessed for each method are the restoration of the static potential's rotational symmetry, as well as agreement between lattice computations of the potential using two discretizations with different static actions. Evidence suggesting the superior efficacy of one of these two methods is presented; an explanation for this discrepancy between methods is proposed and supported by further calculations.

Contents

1 Introduction

In the Standard Model of particle physics, the strong interaction between color-charged elementary particles is described by the theory of Quantum Chromodynamics (QCD). The fundamental local gauge symmetry of QCD, i.e. the invariance of the QCD action under rotations in color space, is characterized by the gauge group SU(3). Therefore, the dynamics of the gauge bosons – the gluons – exhibit self-interactions, a characteristic trait of non-Abelian gauge theories as first described by C. N. Yang and R. L. Mills. [1]
Both the pure Yang-Mills theory of the strong interaction, which omits the presence of dynamical fermions, and full QCD are of great interest in researching the interaction's unique qualities and phenomena; however, a significant challenge to early theoretical descriptions was its eponymous strong coupling below an energy threshold of the order $E \lesssim 1\,\mathrm{GeV}$. [2, 3]
The framework of perturbation theory, which had produced highly successful theoretical predictions in Quantum Electrodynamics (QED) preceding QCD, requires a sufficiently small coupling to allow convergence of power series expansions with respect to this parameter. Thus, non-perturbative methods are necessary to accurately research QCD and obtain physically valid results at lower energy scales.

Lattice gauge theory is a first-principles approach to QCD that regularizes the theory by approximating continuous space-time with a finite, discrete lattice, allowing numerical simulations and theoretical predictions without the inherent restriction to the high-energy sector typical of perturbative analyses. In the past few decades, this approach has been implemented to great success. After the first formulation of QCD on the lattice by K. G. Wilson in 1974 [4], characteristics of the strong interaction such as confinement of quarks and the QCD β-function describing the transition from strong coupling at low energies to asymptotic freedom at high energies could be accurately replicated in lattice simulations using this approach. [4, 5]
In particular, one of the first observables to be successfully described by Wilson's formulation of lattice gauge theory was the potential energy of a quark-antiquark pair as a function of their spatial separation in the static limit (see Sec. 2.1), commonly referred to as the static potential [6]. This quantity – as well as the related static force – continues to be of great interest in QCD research today, due to its relevance to not only improving the theoretical understanding of quark-antiquark pairs themselves, but also to setting the physical scale in lattice QCD [7] and precision computations of observables such as the strong coupling (e.g., [8, 9]).

However, this approach to QCD and Yang-Mills theory gives rise to unwanted effects due to the lattice regularization, the so-called lattice artifacts or discretization errors. For static quark-antiquark pairs on the lattice, these deviations from the expected continuum behavior were first described in the literature soon after the potential itself, becoming apparent in the form of significant breaking of the continuum potential's rotational invariance. [10, 11]
To address this problem, different approaches aiming to reduce discretization errors were proposed, notable examples being two different methods of tree-level improvement [7, 12] specific to the static potential and static force. Here, the lattice data is adjusted in a way that aims to better approximate the continuum counterparts of these observables, which are computed at tree-level of perturbation theory. Due to the nature of perturbative calculations and the strong coupling, this methodology is applicable to the region of small quark-antiquark separations, in which discretization errors are largest.

The first of these methods, which uses a multi-parameter fit procedure discussed in detail in Sec. 4.4, was introduced by C. Michael [12] and has since been commonly used to improve the static potential, see e.g. [13–18].
The second method, often referred to as the method of improved separation, was originally introduced by R. Sommer for the static force [7] and has been used specifically for this quantity

to good success since then, cf. e.g. [15, 19–22]. However, it was later also adopted for the static potential and is still commonly used in this manner, e.g. in Refs. [8, 9, 20, 23–26].

The goal of this thesis is to systematically compare these two methods of tree-level improvement, in particular regarding their efficacy for reducing discretization errors in lattice computations of the static potential. An important result of this is evidence that appears to favor one of the two methods over the other, which is discussed in detail below. Further, an expression aiming to quantitatively explain the problems occurring with the less favorable method is proposed. It is then shown that when adjusting for this term, significantly better restoration of rotational symmetry and agreement between different discretizations can be achieved for the static potential, indicating superior tree-level improvement and supporting the explanation given for the discrepancy between methods.

2 Theory and methodology

In the following, aspects of lattice gauge theory relevant to this thesis are outlined. A more detailed discussion can be found in the introductory literature, see e.g. [27, 28]; the notation used below is primarily based on [27].

Lattice gauge theory allows the numerical evaluation of correlation functions in the path integral formalism by replacing continuous space-time with a finite number of discrete points x on a four-dimensional Euclidean lattice Λ. The four dimensions correspond to the three spatial coordinates $\mathbf{x}$ separated by the lattice spacing a, and Euclidean time t, which is obtained from real time τ by a Wick rotation, $t = i\tau$. Time intervals are commonly discretized with the same lattice spacing a as the spatial components, resulting in a hypercubic lattice structure with volume $T \times L^3$. Here, T and L denote the temporal and spatial extensions of the lattice, respectively.

Due to limited computational capacities, early simulations aiming to investigate the strong interaction in lattice gauge theory (e.g., [4–6]) typically used relatively small lattice volumes and considered Yang-Mills theory with the gauge group SU(2), which describes pure gluodynamics with only two colors. Since then, advancements in technology have been a key driving factor in the progress of lattice gauge theory, allowing increasingly sophisticated simulations. However, since SU(2) Yang-Mills theory accurately describes many of the qualities and characteristic phenomena of full QCD to a reasonable extent, particularly when studying purely gluonic observables such as the static potential, this approach is still a common choice (see e.g. [29–31]) for explorative studies and is used in this work.

In SU(2) lattice gauge theory, the gauge fields of the continuous theory are replaced by link variables $U_\mu(n)$, which are elements of the gauge group SU(2) and connect a given lattice site n to the neighboring lattice site in μ-direction, $n + \hat{\mu}$. In this notation, $n \in \Lambda \subset \mathbb{Z}^4$ describes the lattice sites located at space-time coordinates $x = an$ and $\hat{\mu}$ denotes a unit vector normalized to length a and oriented along one of the lattice axes.

The plaquette $U_{\mu\nu}(n)$ is defined as

$$U_{\mu\nu}(n) = U_\mu(n)\, U_\nu(n+\hat{\mu})\, U_\mu^\dagger(n+\hat{\nu})\, U_\nu^\dagger(n) \tag{1}$$

and forms the smallest non-trivial closed loop of link variables, the trace of which is gauge-invariant due to the transformation properties of the gauge links.

This quantity is key to Wilson's plaquette action [4], a discretization of the continuum SU(N) Yang-Mills action, given by

$$S[U] = \frac{\beta}{N} \sum_{n\in\Lambda} \sum_{\mu<\nu} \mathrm{Re\ Tr}\left(\mathbb{1} - U_{\mu\nu}(n)\right) \ , \tag{2}$$

with $N = 2$ for gauge group SU(2). The inverse coupling β is a quantity commonly used in place of the continuum coupling g in lattice gauge theory and defined as $\beta = \frac{2N}{g^2}$.

It is worth noting that there are other discretizations of the continuum gauge action with different properties, such as the Symanzik improved action [32,33], which – like the methods of tree-level improvement discussed in the following – aims to reduce discretization errors. However, since the focus of this work is tree-level improvement achieved by methods separate from and different to this approach, the standard Wilson plaquette action is used for the lattice calculations of the static potential.

2.1 The static quark-antiquark potential

In the context of the quark-antiquark potential, the static limit is a non-relativistic approximation assuming an infinitely heavy quark and antiquark, which are fixed in space and can neither be dynamically created nor annihilated. Using this approximation, the dependence of path integrals on the static quarks can be "integrated out", allowing calculations of the static potential in pure Yang-Mills theory. [34]

To obtain this observable using lattice gauge theory, it is conducive to first define the Euclidean correlation function

$$C(t) = \langle\Omega|\mathcal{O}^\dagger(t)\mathcal{O}(0)|\Omega\rangle = \frac{1}{Z}\int \mathcal{D}[U]\,\mathcal{O}^\dagger(t)\mathcal{O}(0)\,\mathrm{e}^{-S[U]} \tag{3}$$

of the operator $\mathcal{O}$, which acts on the vacuum state $|\Omega\rangle$ to create a state describing a static quark and antiquark located at two lattice sites separated by the distance r. The partition function Z in the lattice path integral on the right-hand side of Eq. (3) is a normalization factor given by

$$Z = \int \mathcal{D}[U]\,\mathrm{e}^{-S[U]}\ . \tag{4}$$

The static quark-antiquark potential $V(r)$ is defined as the difference between the ground state energy $E_0(r)$ of the quark-antiquark pair at separation r and the energy E_Ω of the vacuum state,

$$V(r) = E_0(r) - E_\Omega\ . \tag{5}$$

This energy difference can be computed by considering the spectral decomposition of the correlation function $C(t)$, which is obtained from Eq. (3) by using a set of energy eigenstates $|n\rangle$ with eigenvalues E_n, and the Euclidean time evolution of the operator $\mathcal{O}$. When considering the limit of large time t, this results in an expression which is exponentially proportional to the static potential:

$$\lim_{t\to\infty} C(t) = \lim_{t\to\infty}\sum_n |\langle n|\mathcal{O}(0)|\Omega\rangle|^2\ \mathrm{e}^{-(E_n(r)-E_\Omega)t} \tag{6}$$

$$= |\langle 0|\mathcal{O}(0)|\Omega\rangle|^2\ \mathrm{e}^{-(E_0(r)-E_\Omega)t}\ \propto\ \mathrm{e}^{-V(r)t}\ . \tag{7}$$

Therefore, the static potential can be obtained by an exponential fit to the correlation function. However, a more commonly used approach is to calculate the static potential from a fit to a constant according to

$$V(r) = \lim_{t\to\infty} V_{\mathrm{eff}}\,(r,t)\ , \tag{8}$$

with the effective potential V_{eff} defined at a given separation r via the dimensionless quantity

$$aV_{\mathrm{eff}}\,(r,t) = \ln\left(\frac{C(t)}{C(t+a)}\right)\Big|_r\ . \tag{9}$$

The t-range of the constant fit has to be chosen carefully in order to avoid unnecessarily large errors due to statistical fluctuations at large t, as well as minimize contributions of excited states, which are exponentially suppressed with increasing t but still contribute significantly if the lower bound of the fit range is chosen too low, cf. Eq. (6). The fitting procedure used in this work is described in more detail in Sec. 3.4.

In practice, the correlation functions $C(t)$ in lattice gauge theory calculations of the static potential are evaluated by calculating the vacuum expectation values of Wilson loops

$$W_{\mathcal{L}}[U] = \mathrm{Tr}\left(\prod_{(k,\mu)\in\mathcal{L}} U_\mu(k)\right) = \mathrm{Tr}\left(\mathcal{S}(\mathbf{m},\mathbf{n},n_t)\,\mathcal{T}^\dagger(\mathbf{n},n_t)\,\mathcal{S}^\dagger(\mathbf{m},\mathbf{n},0)\,\mathcal{T}(\mathbf{m},n_t)\right), \tag{10}$$

which are gauge invariant observables satisfying

$$\lim_{t\to\infty}\langle\Omega|W_{\mathcal{L}}|\Omega\rangle \propto \mathrm{e}^{-V(r)t}\,. \tag{11}$$

In the above definition, the path $\mathcal{L}$ is characterized by two spatial transporters $\mathcal{S}$ and two temporal transporters $\mathcal{T}$ forming a closed loop of gauge links on the lattice.
The temporal transporter $\mathcal{T}(\mathbf{m},n_t)$ is defined as the product of temporal gauge links connecting the lattice points $(\mathbf{m},0)$ and $(\mathbf{m},n_t)$, while $\mathcal{T}^\dagger(\mathbf{n},n_t)$ runs in the opposite temporal direction at spatial coordinates $\mathbf{n}$, connecting the lattice point $(\mathbf{n},n_t)$ to $(\mathbf{n},0)$. Accordingly, the temporal extension T_W of the Wilson loop is given by $T_\mathrm{W} = an_t$.
The spatial transporter $\mathcal{S}(\mathbf{m},\mathbf{n},n_t)$ is analogously defined as a product of gauge links connecting the lattice sites at spatial coordinates $\mathbf{m}$ and $\mathbf{n}$, or vice versa for $\mathcal{S}^\dagger(\mathbf{m},\mathbf{n},0)$, each at a fixed time given by the third argument. The Wilson loop's spatial extension L_W is the parameter defining the quark-antiquark separation r when evaluating the static potential,

$$r = L_\mathrm{W} = a\,|\mathbf{m}-\mathbf{n}|\,. \tag{12}$$

Wilson loops are further categorized by the direction of their spatial paths relative to the lattice. If these paths are defined along a coordinate axis of the lattice and can therefore be described by a straight line of gauge links, they are referred to as on-axis or planar Wilson loops; otherwise, they are termed off-axis or non-planar Wilson loops. The advantage of considering a large number of both on- and off-axis Wilson loops is the possibility to compute a larger data set of the static potential at different separations, with off-axis Wilson loops additionally allowing the evaluation of the potential at non-integer values of r/a.

This is particularly relevant to assessing the restoration of rotational symmetry of the static potential by tree-level improvement. The continuum potential is invariant under spatial rotations of $\mathbf{r} = a\,(\mathbf{m}-\mathbf{n})$, i.e. for different orientations of $\mathbf{r}$ with the same absolute value $r = |\mathbf{r}|$, whereas the lattice potential breaks rotational symmetry due to the discretization of space-time. An example of this are values of the static potential computed from on- and off-axis Wilson loops with the same spatial extension, which correspond to identical values of the continuum potential but frequently differ in lattice calculations, cf. Sec. 4.1.
A more general measure for the restoration of rotational symmetry can be obtained by considering the convergence of a fit of the lattice potential to an appropriate continuum parametrization, effectively giving an indication of how consistent the values from multiple different Wilson loops are with a single curve. A poor fit due to outlying data points, particularly at small quark-antiquark separations, can suggest the presence of discretization errors [10–12].
Thus, fitting the lattice potential to a continuum parametrization also serves as an important tool for assessing the quality of a method of tree-level improvement, cf. e.g. [12, 14, 17], which is discussed in further detail in Sec. 4.

For this purpose, the commonly used parametrization of the static potential is the well-known continuum Cornell potential with an additional additive constant C, given by

$$V(r) = -\frac{\alpha}{r} + \sigma r + C\,. \tag{13}$$

Here, the constant C is included in addition to the Coulomb term with coefficient α and the

linear term proportional to the string-breaking coefficient σ due to a constant, unphysical energy shift that occurs in lattice simulations of the static potential.

2.2 One gluon exchange and the lattice propagator

When evaluated at tree-level of perturbation theory, the continuous static potential describes the one gluon exchange between the quark and the antiquark and has the form of a Coulomb potential inversely proportional to the separation [34],

$$V_{\text{cont}}^{\text{tree-level}}(r) \propto \left(\frac{1}{r}\right)_{\text{cont}} . \tag{14}$$

On the lattice, assuming that one of the static color sources is positioned at the spatial origin and the other at spatial lattice coordinates $\mathbf{R} = \mathbf{r}/a$ resulting in the separation $r = |\mathbf{r}|$, the corresponding one gluon exchange expression is given by the lattice Coulomb potential (see e.g. [10, 12, 35])

$$V_{\text{lat}}^{\text{tree-level}}(r) \propto \left(\frac{1}{r}\right)_{\text{lat}} = \frac{4\pi}{a}\, G(\mathbf{R})\,. \tag{15}$$

The lattice propagator $G(\mathbf{R})$ in position space is given by the Green's function

$$G_{\text{EH}}(\mathbf{R}) = \frac{1}{(2\pi)^3} \int_{-\pi}^{\pi} \frac{\prod_{j=1}^{3} \cos(p_j R_j)}{\sum_{j=1}^{3} 4\sin^2(p_j/2)}\, \mathrm{d}^3 p \tag{16}$$

for computations using the Wilson plaquette gauge action and the Eichten-Hill (EH) static action, cf. e.g. [17, 18]. The latter refers to the standard action for static quarks introduced by E. Eichten and B. Hill [36], which uses unsmeared temporal gauge links as opposed to the HYP static action, see [17, 37–39]. The HYP smearing of temporal links is characterized by the parameters α_1, α_2 and α_3 and will be discussed further in Sec. 3.1. For the lattice propagator, the use of the HYP static action requires the multiplication of the integrand in Eq. (16) by an additional factor [17], resulting in

$$G_{\text{HYP}}(\mathbf{R}) = \frac{1}{(2\pi)^3} \int_{-\pi}^{\pi} \frac{\prod_{j=1}^{3} \cos(p_j R_j) \cdot \left(1 - (2\alpha_1/3) \sum_{i=1}^{3} \sin^2(p_i)\, \Omega_{i0}(p)\right)^2}{\sum_{j=1}^{3} 4\sin^2(p_j/2)}\, \mathrm{d}^3 p\ , \tag{17}$$

with $\Omega_{\mu\nu}$ defined as

$$\begin{aligned} \Omega_{\mu\nu}(p) = {} & 1 + \alpha_2(1+\alpha_3) - \alpha_2(1+2\alpha_3) \left(\sum_{j=1}^{3} \sin^2(p_j/2) - \sin^2(p_\mu/2) - \sin^2(p_\nu/2)\right) \\ & + \alpha_2\alpha_3 \prod_{\eta\neq\mu,\nu} \sin^2(p_\eta/2)\ . \end{aligned} \tag{18}$$

The lattice propagator for the Eichten-Hill static action was calculated using a recursion relation discussed in Refs. [20, 40]. For the HYP static action, the values were obtained numerically via Monte Carlo integration in the context of Ref. [18].

3 Computational details

3.1 Lattice setup and gauge link smearing

The calculations of the static potential presented in the following were performed in SU(2) lattice gauge theory using the Wilson plaquette gauge action and a lattice with temporal and spatial extensions $T/a = L/a = 16$. The inverse coupling set to $\beta = 2.40$ corresponds to a lattice spacing of approximately $a \approx 0.097\,\text{fm}$ when introducing physical units via the Sommer scale [7] with the Sommer parameter $r_0 = 0.5\,\text{fm}$, cf. Sec. 4.5.

In total, 20 000 gauge link configurations were generated for this work using an SU(2) heat bath algorithm. Each sweep of this Markov chain Monte Carlo algorithm describes an update of every gauge link on the lattice according to a statistical heat bath probability distribution depending on the gauge action, cf. e.g. [6,27]. After a hot start, which refers to the initialization of the gauge links to random SU(2) matrices, 1 000 thermalization sweeps were performed to ensure that the following configurations are sufficiently close to the equilibrium distribution. To measure observables accurately, these thermalization updates are discarded. Further, the configurations used to compute the expectation values of Wilson loops are each separated by 100 sweeps in order to reduce statistical correlations between subsequent configurations.
Consequently, 190 of the generated gauge link configurations were used to measure the static potential for each of the two computations described in the following.

As mentioned in Sec. 2.2, one of these two calculations of the static potential uses the Eichten-Hill static action with unsmeared temporal links (abbreviated as the *"no-HYP"* computation in the following), while the other uses the HYP2 static action (*"HYP2"* computation).
Generally, the HYP static action is characterized by the hypercubic smearing of temporal gauge links, in which these link variables are replaced by an average over paths within the hypercubes attached to the respective original gauge link, cf. [17, 37, 38].
The specification HYP2 refers to the choice of smearing parameters $\alpha_1 = 1.0$, $\alpha_2 = 1.0$, and $\alpha_3 = 0.5$, which approximately minimizes the noise-to-signal ratio and the unphysical self-energy shift in lattice computations [39, 41], thereby significantly reducing statistical errors. However, a disadvantage of HYP smearing for the static potential is the occurrence of increased discretization errors at small separations [17], appearing in the form of noticeable distortions of the short distance potential, cf. Sec. 4.

Besides the smearing applied to the temporal gauge links for the *HYP2* computation, both computations in this work use APE smearing [42] for the spatial links with $N_{\text{APE}} = 20$ steps and $\alpha_{\text{APE}} = 0.5$, which is a commonly used choice of parameters, cf. e.g. [43]. This technique replaces a given gauge link with the weighted average of the original link itself and its six orthogonal staples, which are each products of the three gauge links that form a path connecting the endpoints of the original gauge link [27]. The benefit of APE smearing is an increased overlap of the trial state generated by the operator $\mathcal{O}$ (cf. Sec. 2.1) with the ground state of the static potential, allowing a more precise extraction of the potential due to an improved signal-to-noise ratio, see e.g. [44].

3.2 On- and off-axis Wilson loops

The typical vector notation (see e.g. [12–15, 45]) for a Wilson loop is defined by the difference between its spatial start- and endpoint in lattice coordinates, $(x/a,\, y/a,\, z/a) = \mathbf{m} - \mathbf{n}$. This description is irrespective of the exact orientation of the spatial paths – for example, no distinction is made between $(1, 0, 0)$ and $(0, 1, 0)$, since these are both on-axis Wilson loops resulting in

the same separation and are therefore typically averaged together as described in the following. However, it should be stressed in the context of this thesis that an explicit distinction is made between different spatial paths only resulting in the same separation, such as the on-axis Wilson loop $(3,0,0)$ and the off-axis Wilson loop $(2,2,1)$, since these can result in slightly different values of the lattice static potential due to the breaking of rotational symmetry, cf. Sec. 2.1.

To obtain the static potential, the vacuum expectation values of Wilson loops were averaged over 190 gauge link configurations, cf. Sec. 3.1, and evaluated as described in Sec. 2.1. Further, the average over three orthogonal spatial directions, each parallel to the lattice axes, was taken for all on-axis Wilson loops to improve statistics. Similarly, the expectation values of the off-axis Wilson loops were each averaged over four of the possible different orientations of the spatial transporters, namely the directions $(1,1,0)$, $(1,-1,0)$, $(1,0,-1)$ and $(1,0,1)$ for the two-dimensional off-axis Wilson loops, as well as the directions $(1,1,1)$, $(1,-1,-1)$, $(1,-1,1)$ and $(1,1,-1)$ for the three-dimensional off-axis Wilson loops. This choice does not exhaust all of the possible spatial directions in order to save computation time, while still helping to reduce statistical errors.

Off-axis Wilson loops require the implementation of spatial transporters diagonal to the gauge links. To obtain two-dimensional diagonal paths of the form $\mathbf{r}/a = (1,1,0)$, the sum S of two products of gauge links, which describe the two L-shaped paths connecting the diagonal's start- and endpoint along the lattice axes, is computed and the result is projected back to SU(2) with

$$P_{\mathrm{SU}(2)}\, S = \frac{1}{\sqrt{\det\left(S\right)}}\, S\,. \tag{19}$$

Three-dimensional diagonal links of the form $\mathbf{r}/a = (1,1,1)$ are constructed analogously as an average over the six possible paths that connect its start- to its endpoint and are each built from the product of three gauge link variables.

The Wilson loops used for the computation of the static potential in this thesis, given in vector notation as described above, are

$$\begin{aligned}
&\mathbf{r}/a = n\,(1,0,0)\,, && n \in \{0,1,\ldots,8\},\\
&\mathbf{r}/a = n\,(1,1,0)\,, && n \in \{1,2,3\},\\
&\mathbf{r}/a = n\,(1,1,1)\,, && n \in \{1,2,3\},\\
&\mathbf{r}/a = (n,1,0)\,, && n \in \{2,3,4\},\\
&\mathbf{r}/a = (n,1,1)\,, && n \in \{2,3,4\},\\
&\mathbf{r}/a = (n,n,1)\,, && n \in \{2,3\},\\
&\mathbf{r}/a = (3,2,n)\,, && n \in \{0,1,2\},\\
&\mathbf{r}/a = (4,3,0)\,,\\
&\mathbf{r}/a = (3,3,2)\,.
\end{aligned}$$

The first row corresponds to the on-axis Wilson loops, while all further rows describe the off-axis Wilson loops considered. The maximum spatial and temporal extension of the Wilson loops is $L_{\mathrm{W,max}} = T_{\mathrm{W,max}} = 8a$, since the inclusion of too large extensions can introduce additional systematic errors due to the finite size of the lattice, cf. e.g. [6].
The total number of different Wilson loops computed for each static action is 28, which includes a total of 19 off-axis Wilson loops in the separation range $\sqrt{2} \leq r/a \leq 3\sqrt{3}$, allowing the study of discretization errors and rotational symmetry of the static potential at small separations in detail.

3.3 Statistical errors

All statistical errors cited in this work were obtained via a Jackknife analysis, which is a commonly used tool for the statistical analysis of large data sets. While the equations particularly relevant to this thesis are briefly described below, a more detailed discussion of this method can be found in the literature, see e.g. [46].

Given a set of N data points θ_j $(j = 1, \ldots, N)$ describing a quantity θ (e.g., the static potential at a fixed separation), N so-called Jackknife samples specified by the index $n = 1, \ldots, N$ are constructed from the original set by omitting the n-th data point, respectively.
The mean of the full data set $\overline{\theta}$ and the mean of each Jackknife sample $\overline{\theta_n}$ is calculated using the standard arithmetic average

$$\overline{\theta} = \frac{1}{N} \sum_{j=1}^{N} \theta_j \ , \tag{20}$$

$$\overline{\theta_n} = \frac{1}{N-1} \sum_{\substack{j=1 \\ j \neq n}}^{N} \theta_j \ . \tag{21}$$

Then, the Jackknife estimate for the standard deviation $\sigma(\theta)$, which defines the statistical errors quoted in the following in the form of $\overline{\theta} \pm \sigma(\theta)$, is given by

$$\sigma(\theta) = \sqrt{\frac{N-1}{N} \sum_{n=1}^{N} \left(\overline{\theta_n} - \overline{\theta}\right)^2} \ . \tag{22}$$

3.4 Fitting procedure

Both the extraction of the static potential from the effective potential as described in Sec. 2.1 and the comparison of methods of tree-level improvement discussed in the following in Sec. 4 require the fitting of lattice data to a given function while taking statistical errors into consideration. For this purpose, the method of χ^2-minimizing fitting was employed, which is outlined below; further details are described in e.g. [47, 48].

This approach aims to approximate a set of N data points $f_j(x_j)$ $(j = 1, \ldots, N)$ with respective errors σ_j by using a fit ansatz $g(x_j; \mathbf{a})$ depending on M fit parameters, $\mathbf{a} = (a_1, \ldots, a_M)$.
To achieve an optimal fit, the weighted squared difference

$$\chi^2 = \sum_{j=1}^{N} \left(\frac{g(x_j; \mathbf{a}) - f_j}{\sigma_j} \right)^2 \tag{23}$$

between the fit function and data points is minimized by a suitable choice of fit parameters determined by solving

$$\nabla^{(\mathbf{a})} \chi^2 = 0 \ . \tag{24}$$

The value of χ^2 per degree of freedom ($d.o.f.$), or reduced χ^2, is given by

$$\chi^2_{\text{red}} = \frac{\chi^2}{d.o.f.} = \frac{\chi^2}{N - M} \tag{25}$$

and provides an indication of the quality of a fit, with $\chi^2_{\text{red}} \approx 1$ being considered ideal. A much lower result $\chi^2_{\text{red}} \ll 1$ potentially points to problems such as correlated data points or overestimation of errors, while a considerably higher value of $\chi^2_{\text{red}} \gg 1$ indicates poor consistency

of the data with the chosen fit function, or in some cases the presence of additional error sources which were not accounted for in the specified values of σ_j. The latter will be particularly relevant to the discussion of systematic lattice discretization errors of the static potential in the following.

In the special case of a one-parameter fit to a constant, $g(a) = a$, finding the constant a that minimizes χ^2 is equivalent to calculating the weighted sum

$$a = \sum_{j=1}^{N} w_j f_j \ , \tag{26}$$

with the weight factors $w_j \in [0, 1]$ defined as

$$w_j = \frac{1/\sigma_j^2}{\sum_{k=1}^{N} 1/\sigma_k^2} \ . \tag{27}$$

This method was used to obtain the static potential by approximating plateaus of the effective potential as described in Sec. 2.1, using a fixed fit range of $3 \leq t/a \leq 7$.

The three- and four-parameter fits of the static potential discussed in Sec. 4 require the fitting of data points to parametrizations that are linear in the fit parameters. In this case, Eq. (24) yields a system of linear equations, which was solved using Gaussian elimination with back substitution and scaled partial pivoting to obtain the fits presented in this work.

4 Tree-level improvement of the static potential

The goal of tree-level improvement is to reduce discretization errors in lattice gauge theory computations of the static potential and static force, which occur due to the lattice regularization of continuous space-time. In the following, two commonly used methods of tree-level improvement are examined in detail for the static potential. In order to illustrate the aforementioned discretization errors and establish a baseline for later comparison, the lattice static potential without the use of tree-level improvement is discussed first.

4.1 The unimproved potential

The lattice results for the unimproved static potential of both the *no-HYP* and *HYP2* computations performed in this work, cf. Sec. 3.1, are presented in Fig. 1 in lattice units, i.e. in terms of the dimensionless quantities r/a for the separation r and aV for the potential V. The advantage of this representation is that it does not require an additional scale setting step to determine the lattice spacing a in physical units (cf. e.g. [7, 49]), since r/a and aV directly correspond to the quantities processed by the computer in lattice gauge theory computations of the static potential. This avoids the risk of introducing additional error sources through setting the scale, which is particularly high in the presence of discretization errors.

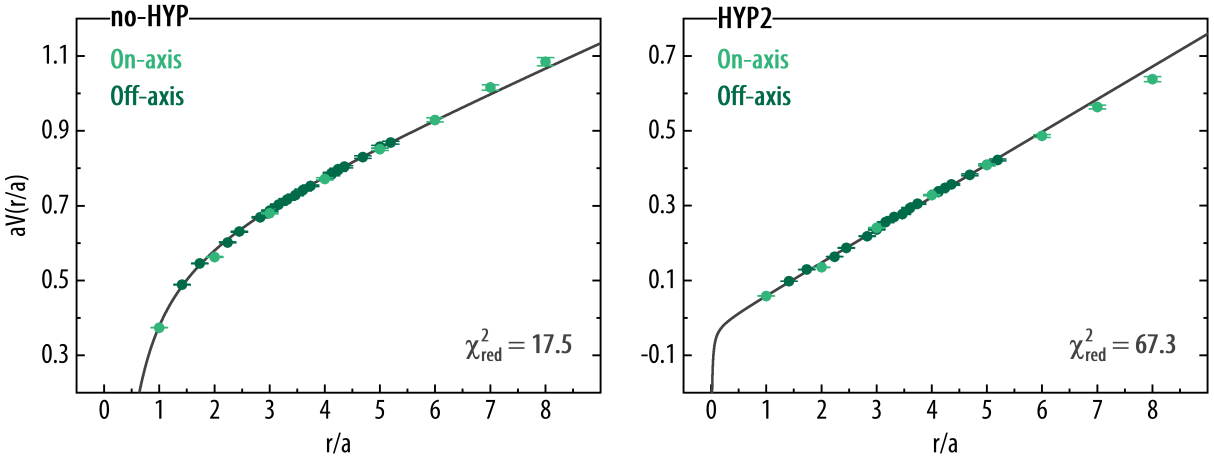

Figure 1: *Results of lattice computations of the static potential using the Eichten-Hill (*"no-HYP"*) or HYP2 (*"HYP2"*) static action without tree-level improvement. Data points obtained by on-axis and off-axis Wilson loops are indicated by their light green and dark green color, respectively. The fit to the Cornell plus constant parametrization and the resulting reduced χ^2 of the fit are shown in dark grey.*

The fit functions shown in Fig. 1 were each obtained by three-parameter χ^2-minimizing fits to the continuum Cornell potential with an additional constant, cf. Eq. (13), in lattice units. This is also referred to as the lattice Cornell parametrization in the following and given by

$$aV\left(\frac{r}{a}\right) = -\alpha \cdot \left(\frac{r}{a}\right)^{-1} + a^2\sigma \cdot \frac{r}{a} + aC\,. \tag{28}$$

The three dimensionless fit parameters are the Coulomb coefficient α, the string breaking coefficient in lattice units $a^2\sigma$, and the constant aC describing lattice artifacts including the self-energy of the static quarks; the results for these parameters are collected in Table 1.

The reduced self-energy of the *HYP2* computation of the potential in comparison to the *no-HYP* computation using the Eichten-Hill static action, cf. Sec. 3.1, is the reason for the constant shift between the y-axes in Fig. 1.

The discretization errors present in the unimproved lattice potential are readily apparent in Fig. 1, exemplifying the necessity of tree-level improvement. The *HYP2* values in particular visibly deviate from the typical shape of a Cornell potential, which is empirically expected to be a suitable parametrization for the continuum potential.
More specifically, the breaking of rotational symmetry is visible in both the *no-HYP* and *HYP2* computations of the potential, most notably in the region of small quark-antiquark separations. A clear indication of this is the poor fit convergence seen in both data sets, with values of $\chi^2_{\text{red}} = 17.5$ for the *no-HYP* computation and $\chi^2_{\text{red}} = 67.3$ for the *HYP2* computation strongly suggesting the presence of discretization errors, cf. Sec. 2.1. It should be noted that fits of the static potential are typically restricted to separations greater than approximately $r/a \gtrsim 2 - 3$ for just this reason, cf. e.g. [22, 24, 26]. However, for the purposes of this work, all separations $1 \leq r/a \leq 8$ are specifically included in the fit range in order to examine and compare discretization errors at small separations.
Illustrative examples showing the lack of rotational symmetry are the two data points at separation $r/a = 3$ in the *no-HYP* results. Here, the static potential is computed separately by both an on-axis and an off-axis Wilson loop (see Sec. 3.2), which return slightly different results despite corresponding to the same separation, in contrast to the rotationally invariant continuum potential. Similar observations can be made for the data points at separation $r/a = 5$ of the *no-HYP* potential and, somewhat more subtly, $r/a = 3$ of the *HYP2* potential.

Another important point of reference for the size of discretization errors in lattice calculations of the static potential is the level of agreement between different discretizations. This can, for example, be assessed by comparing computations using different static actions, such as the *no-HYP* and *HYP2* discretizations discussed in this thesis. An alternative option is the use of multiple different lattice spacings, see e.g. [18].
In an idealized case without any discretization errors, the results for the potential and thus, the variables α and $a^2\sigma$ defining its fit function in the lattice Cornell parametrization, should not depend on the particular discretization used. However, a comparison between the *no-HYP* and *HYP2* fit parameters listed in Table 1 shows that for the unimproved potential, these parameters do not match between discretizations, even when taking statistical errors into account.
This is expected for the constant shift aC due to the decreased self-energy of the static quarks in the *HYP2* computation, but the differences between the *no-HYP* and *HYP2* values of both α and $a^2\sigma$ show a dependence on the discretization that is indicative of lattice artifacts.

	$\boldsymbol{\alpha}$	$\boldsymbol{a^2\sigma}$	$\boldsymbol{aC}$
no-HYP	0.277 ± 0.009	0.064 ± 0.011	0.59 ± 0.06
HYP2	0.003 ± 0.04	0.087 ± 0.006	-0.03 ± 0.04

Table 1: *Parameters computed by a χ^2-minimizing three-parameter fit of the unimproved static potential to the lattice Cornell parametrization with fit range $1 \leq r/a \leq 8$.*

A comparison of the *no-HYP* and *HYP2* values of the unimproved potential is shown in Fig. 2. To allow a direct comparison between these discretizations despite the difference in the self-energy, the respective constants $(aC)'$ have been subtracted from the potential in both data sets. Here and in the following sections, the prime in $(aC)'$ indicates that these constants have been obtained by fits with restricted separation ranges, as opposed to the constants aC deter-

mined by the original fits including all separations. The ranges of these additional fits are limited to larger separations, starting from $r/a \geq 3-5$ depending on the static action and improvement method, to obtain sufficiently precise values for the constants with fewer distortions caused by discretization errors.
Fig. 2 shows a clear discrepancy between the *no-HYP* and *HYP2* data points at small separations $r/a \lesssim 2$, in accordance with this being the range in which discretization errors are known to be largest. Similarly to the comparison of the fit parameters discussed above, this illustrates an unphysical dependence of the unimproved lattice potential on the static action at these separations.

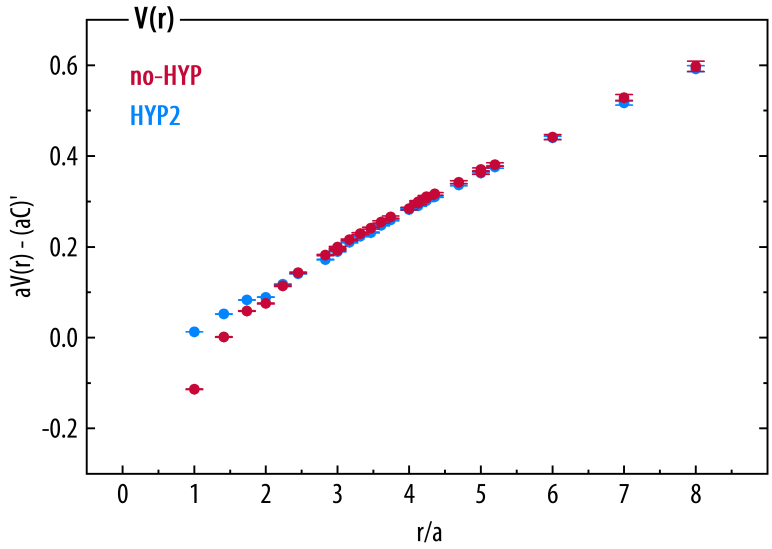

Figure 2: *Direct comparison of the* no-HYP *and* HYP2 *computations of the unimproved static potential. The unphysical constant shifts* $(aC)'_{no\text{-}HYP} = 0.49$ *and* $(aC)'_{HYP2} = 0.05$ *have been subtracted to aid comparison.*

The methods of tree-level improvement discussed below aim to address the problems presented in this section and achieve results that reflect the expected behavior of the continuum potential more closely. In the following, the methods are compared by assessing the same criteria as described above, i.e. the achieved degree of rotational symmetry and the level of agreement between the *no-HYP* and *HYP2* values of the potential and its parameters α and $a^2\sigma$.

4.2 The method of improved separation: $V(r_{\mathrm{impr}})$

The method of improved separation for the static potential, also abbreviated as r-improvement in the following, is a method of tree-level improvement that replaces the separation r of the unimproved potential with the so-called improved separation r_{impr} for all data points, $V(r) \to V(r_{\mathrm{impr}})$. While the original separations of the unimproved potential are simply given by $r = |\mathbf{r}|$, where $\mathbf{r}$ describes the spatial paths of the respective Wilson loops (cf. Sec. 3.2), the definition of the improved separation is motivated by tree-level perturbative calculations of the static potential. Specifically, it is defined according to the lattice one gluon exchange expression, cf. Eq. (15), as

$$\frac{r_{\mathrm{impr}}}{a} = \frac{1}{4\pi\, G(\mathbf{r}/a)} \quad . \tag{29}$$

Here, the values of the lattice propagator $G(\mathbf{r}/a)$ have to be determined separately for the *no-HYP* and *HYP2* computations, since the definition differs between the Eichten-Hill and the HYP static action, cf. Sec. 2.2.

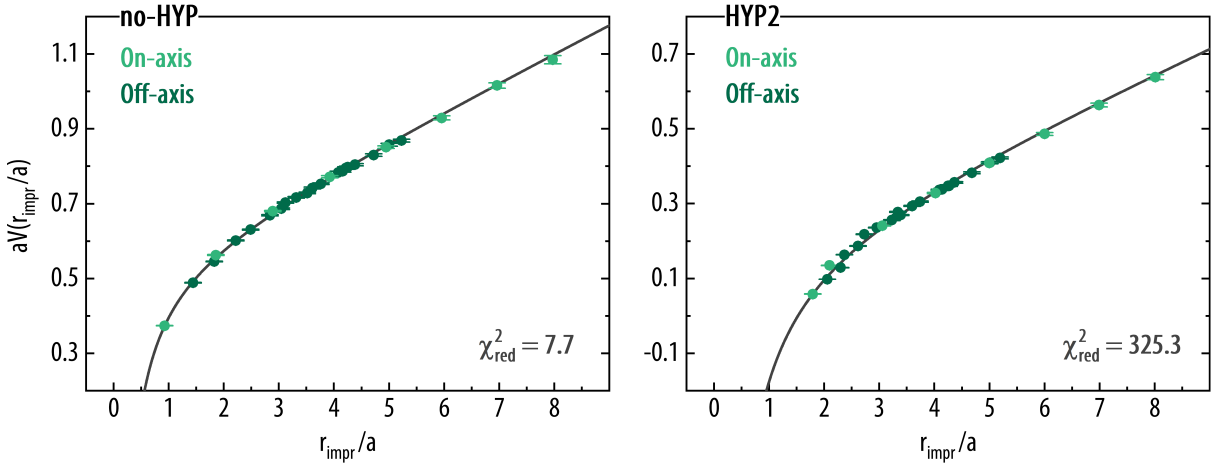

Figure 3: *Results for the r-improved static potential from the* no-HYP *and* HYP2 *computations with three-parameter fits to the lattice Cornell parametrization.*

Fig. 3 shows the results of this method of tree-level improvement for the *no-HYP* and *HYP2* static potential computed in this work. As discussed in Sec. 2.1, the convergence of a fit of the potential to an appropriate parametrization serves as an indicator for the quality of a method of tree-level improvement, since it provides a measure for the restoration of rotational symmetry. Ideally, the data points should be consistent with a single, smooth curve; however, noticeable deviations of the r-improved potential from the fit functions parametrized by the lattice Cornell potential are still visible in Fig. 3, particularly at small separations.

The fit convergence of the *no-HYP* computation is moderately improved as indicated by a lower – though still not ideal – value of $\chi^2_{\text{red}} = 7.7$, which suggests that a certain degree of restoration of rotational symmetry could be achieved for this discretization. This is also evident in Fig. 3, as the values of the r-improved potential computed by on- and off-axis Wilson loops are slightly more consistent than those of the unimproved potential shown in Fig. 1.
However, the result $\chi^2_{\text{red}} = 325.3$ for the *HYP2* computation shows a fit convergence that is considerably worse than even that of the unimproved potential, suggesting a severe lack of rotational symmetry. This is reflected in the corresponding graph: despite the overall shape of the r-improved potential resembling the typical Cornell potential more closely at first glance, the discrepancy between on- and off-axis data points is noticeably more pronounced at small separations $r_{\text{impr}}/a < 3$ when compared to the unimproved *HYP2* potential.

	α	$a^2\sigma$	aC
no-HYP	0.21 ± 0.05	0.075 ± 0.006	0.53 ± 0.04
HYP2	0.41 ± 0.15	0.065 ± 0.018	0.17 ± 0.11

Table 2: *Fit parameters obtained by χ^2-minimizing fits of the r-improved static potential to the lattice Cornell parametrization. The fit ranges each include all values of r_{impr}/a.*

When comparing the *no-HYP* and *HYP2* computations of the r-improved static potential, the respective values α and $a^2\sigma$ given in Table 2 narrowly match within their statistical errors, in contrast to the unimproved potential. However, it should be noted that these errors are significantly larger than the corresponding errors of the unimproved potential, particularly for the *HYP2* computation due to the poor fit. A more illuminating point of reference less affected by large statistical errors is therefore a direct comparison between the values of the potential, which is shown in Fig. 4.

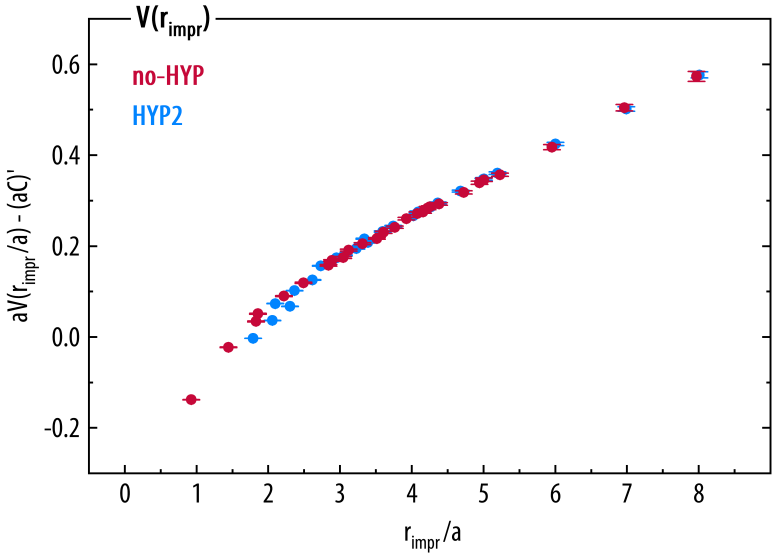

Figure 4: *Comparison of the* no-HYP *and* HYP2 *static potential as a function of the improved separation* r_{impr} *with the constant shifts* $(aC)'_{no\text{-}HYP} = 0.51$ *and* $(aC)'_{HYP2} = 0.06$ *subtracted.*

Here, a distinct discrepancy between the *no-HYP* and *HYP2* computations arises again at small separations $r_{\text{impr}}/a \lesssim 3$. While the deviation between the values of the potential appears slightly smaller than for the unimproved potential, see Fig. 2, these visible discretization errors extend to larger separations here than for the latter, where they are only prominent for $r/a \lesssim 2$.

Furthermore, Fig. 4 shows signs of an "overcorrection" of the static potential by the method of improved separation, which is discussed in detail in the following section. When comparing this graph with Fig. 2, it is noticeable that the sign of the difference between the *no-HYP* and *HYP2* values of the potential (minus the unphysical constant $(aC)'$) is flipped: after r-improvement, the *HYP2* computation returns lower values at small separations than the *no-HYP* computation, while the opposite is the case for the unimproved potential.
This observation in combination with the considerably worse fit convergence of the *HYP2* data points suggests that this issue of overcorrecting the potential lies with these values in particular.

4.3 The method of improved separation with a linear correction: $V_{\text{corr}}(r_{\text{impr}})$

To find an explanation for the problems discussed in the previous section, it is necessary to examine the improved separation r_{impr}, as well as the commonly used definition of the improvement step $V(r) \to V(r_{\text{impr}})$, more closely.

The method of improved separation was originally introduced for tree-level improvement of the static force [7]. Similarly to the definition of r_{impr} for the static potential, cf. Eq. (29), the improved separation r^F_{impr} for the static force $F(r)$ along the orientation $\mathbf{d}$ is given by an

expression characterized by the lattice propagator $G(\mathbf{r})$,

$$r_{\text{impr}}^{F} = \left(\frac{|\mathbf{d}|}{4\pi \left(G\left(\mathbf{r}/a\right) - G\left((\mathbf{r}-\mathbf{d})/a\right)\right)} \right)^{1/2} \quad . \tag{30}$$

Improvement is then achieved by replacing the separation r with r_{impr}^{F}, which results in values $F(r_{\text{impr}}^{F})$ that are in agreement with the continuum force at tree-level of perturbation theory,

$$F(r) \propto \frac{1}{r^2} \quad \rightarrow \quad F(r_{\text{impr}}^{F}) \propto \frac{1}{(r_{\text{impr}}^{F})^2} \quad . \tag{31}$$

Consequently, $F(r_{\text{impr}}^{F})$ is a tree-level improved observable; for further details, see Ref. [7].

For the static potential, the equivalent replacement of the separation r by the improved separation r_{impr} can be described in a similar manner as

$$V(r) = -\frac{\alpha}{r} + \sigma r + C \quad \rightarrow \quad V(r_{\text{impr}}) = -\frac{\alpha}{r_{\text{impr}}} + \sigma r_{\text{impr}} + C \ . \tag{32}$$

The tree-level perturbative expression for the lattice static potential describes one gluon exchange in terms of the lattice Coulomb potential, cf. Sec. 2.2. The method of improved separation takes this into account by replacing $\frac{\alpha}{r}$ with $\frac{\alpha}{r_{\text{impr}}}$.
However, since the linear term proportional to the string breaking coefficient σ is a non-perturbative component of the static potential in Yang-Mills theory and QCD, there appears to be no similar theoretical basis for replacing the separation in this term by an expression r_{impr} that is inherently based on tree-level perturbative calculations.

Thus, the replacement $\sigma r \rightarrow \sigma r_{\text{impr}}$ that occurs within the definition of the r-improved static potential $V(r_{\text{impr}})$ is a plausible possible explanation for the overcorrection observed above. This can be quantified by defining an "overcorrection term"

$$\Delta = \sigma \left(r_{\text{impr}} - r \right), \tag{33}$$

with the proposed corrected expression for the r-improved static potential being

$$V_{\text{corr}}(r_{\text{impr}}) = V(r_{\text{impr}}) - \Delta = -\frac{\alpha}{r_{\text{impr}}} + \sigma r + C \ . \tag{34}$$

Detailed evidence for this hypothesis is explored in the following. Beyond this, it is also supported by numerical tests performed in the context of Ref. [18], which suggest that the aforementioned problems do not occur in a similar manner for the static force, in accordance with this observable not including the non-perturbative linear term σr.

Further, this explanation is highly consistent with the specifics of the overcorrection observed in the previous section, in regards to this problem being the most pronounced for the *HYP2* potential at small separations.
In Fig. 5, the difference between the improved and unimproved separations $(r_{\text{impr}} - r)$, which is proportional to the overcorrection term Δ proposed above, is plotted as a function of the original separation r in lattice units. Here, it is not only apparent that this term gets noticeably larger for small separations, but also that the difference is particularly large for the *HYP2* discretization. This is due to the distortion of the static potential at small separations caused by HYP smearing, cf. [17]. In the context of the r-improved potential, this provides a coherent explanation for both the remarkably poor fit convergence of the *HYP2* potential, cf. Fig. 3, and the larger overcorrection of these data points observed by comparing Figs. 2 and 4.

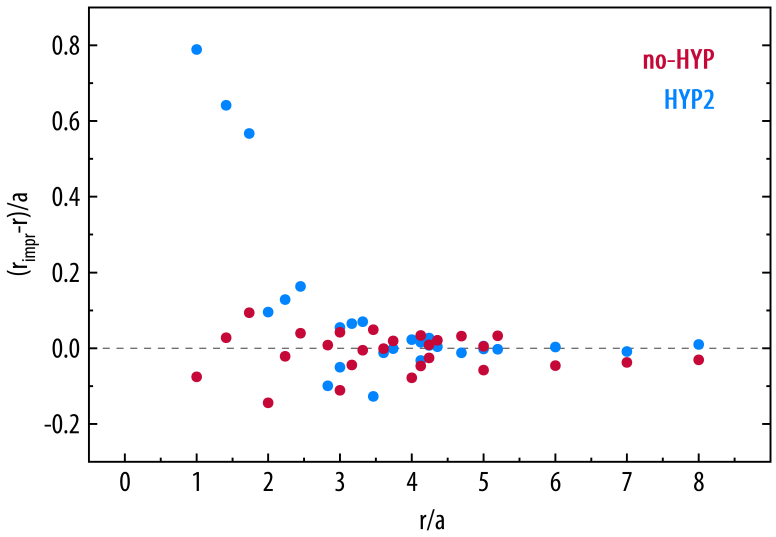

Figure 5: *Difference between the improved separation* r_{impr} *and the unimproved separation* r *in lattice units as a function of* r/a *for the* no-HYP *and* HYP2 *discretizations. The separations included in this graph correspond to the Wilson loops computed in this thesis, cf. Sec. 3.2.*

The results for the r-improved potential with the linear correction defined in Eqs. (33) and (34) are presented in Fig. 6 in lattice units.
To obtain the values $aV_{\text{corr}}(r_{\text{impr}}/a)$, the term $a\Delta = (a^2\sigma)' \cdot (\frac{r_{\text{impr}}}{a} - \frac{r}{a})$ was subtracted from the values of the potential $aV(r_{\text{impr}}/a)$. Similarly to the notation of the constants $(aC)'$, the prime in the coefficient $(a^2\sigma)'$ indicates that this value was computed using a reduced fit range in order to obtain a more accurate result. Specifically, $(a^2\sigma)'$ was determined by a fit of the r-improved *HYP2* potential to the lattice Cornell parametrization with the restriction $r_{\text{impr}}/a \geq 5$. This separation range is chosen to avoid the discretization errors at shorter distances, while the *HYP2* computation is a suitable choice due to the smaller statistical errors. Further, there is little difference between r_{impr} and r for the *HYP2* potential in this region, cf. Fig. 5. This is an important consideration to prevent an interdependence between the result for $(a^2\sigma)'$ and the proposed overcorrection itself, since the latter affects the fitted data points $aV(r_{\text{impr}}/a)$ less for smaller values of $\Delta \propto (r_{\text{impr}} - r)$.

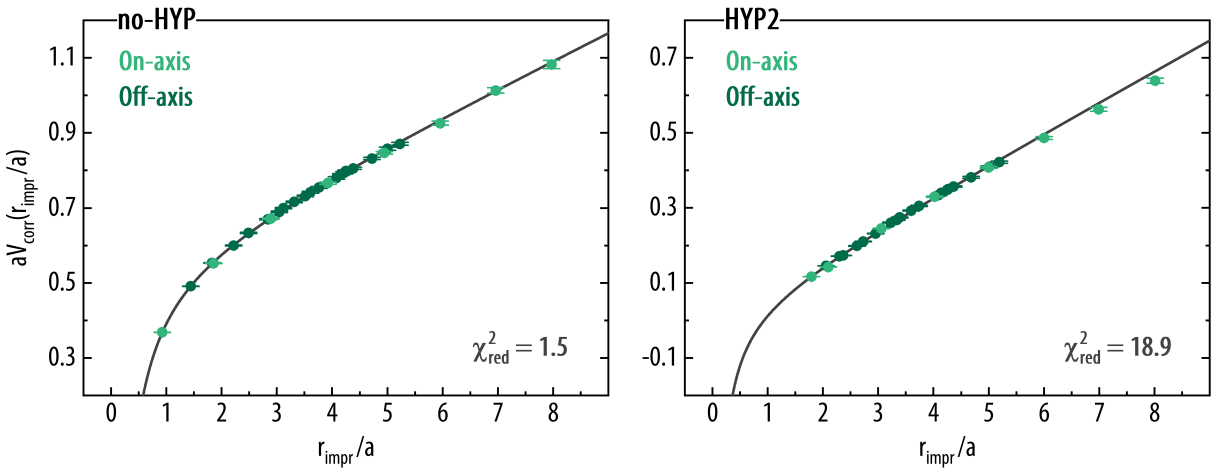

Figure 6: *The corrected* r*-improved static potential from the* no-HYP *and* HYP2 *computations with three-parameter fits to the lattice Cornell parametrization.*

When comparing Fig. 6 to the equivalent graph without the correction of the potential, see Fig. 3, the most immediately noticeable difference is the substantially improved rotational symmetry of the corrected potential. The fit convergence of the data points from the *no-HYP* computation is close to ideal, as indicated by the value of $\chi^2_{\text{red}} = 1.5$. Additionally, while the result $\chi^2_{\text{red}} = 18.9$ for the *HYP2* potential is not optimal by usual standards, it is an immense improvement compared to the previous value of $\chi^2_{\text{red}} = 325.3$ for the r-improved potential before the linear correction.

	α	$a^2\sigma$	aC
no-HYP	0.222 ± 0.013	0.0720 ± 0.0019	0.542 ± 0.011
HYP2	0.09 ± 0.06	0.082 ± 0.006	0.02 ± 0.04

Table 3: *Fit parameters of χ^2-minimizing fits of the corrected r-improved static potential to the lattice Cornell parametrization. All separations r_{impr}/a are included in the fit ranges.*

Furthermore, after correcting the values of the potential, the statistical errors of the fit parameters are less than half of those computed for the improved separation method alone, see Tables 2 and 3. In accordance with the much improved fit convergence of the full data set discussed above, this indicates more consistent fits across the Jackknife samples (cf. Sec. 3.3). However, as a consequence, the parameters α and $a^2\sigma$ no longer match between the *no-HYP* and *HYP2* computations within their statistical errors, despite the discrepancy being smaller in absolute terms than that between the corresponding parameters of the r-improved potential without the correction.

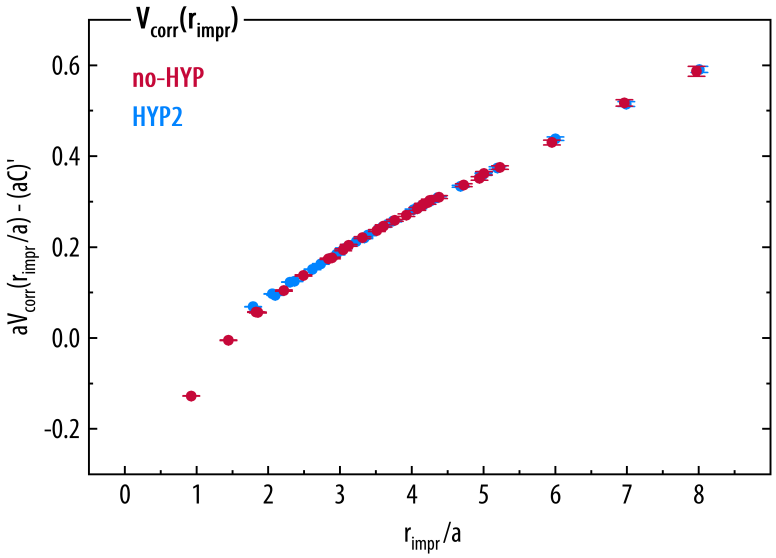

Figure 7: *Comparison between the results for the corrected r-improved static potential in the* no-HYP *and* HYP2 *discretizations. The values of the subtracted constants are given by $(aC)'_{no\text{-}HYP} = 0.50$ and $(aC)'_{HYP2} = 0.05$.*

A more conclusive observation can be made by comparing Fig. 7, showing the direct comparison between the *no-HYP* and *HYP2* computations of the corrected r-improved potential, to Fig. 4, which shows the same comparison without the correction.

It is readily apparent in these graphs that the corrected potential shows significantly better agreement between the two discretizations. Along with the highly improved restoration of rotational symmetry achieved by accounting for the correction term, this strongly supports the proposed explanation for the problems occurring with the method of improved separation.

4.4 Improvement using a four-parameter fit: $V_{\mathbf{impr}}(r)$

The method of tree-level improvement discussed in the following is based on a multi-parameter fit of the lattice static potential and is also referred to as V-improvement below. The starting point of this method is the definition of a fit function for the potential that aims to isolate the contributions stemming from lattice artifacts into separate terms. While this was achieved by a five-parameter fit in the original definition of the method, see Ref. [12], the parametrization considered in this thesis is given by the commonly used four-parameter fit function

$$V(r) = -\frac{\alpha}{r} + \sigma r + C + \tilde{\alpha}\left(\frac{1}{r} - \frac{4\pi G(\mathbf{r}/a)}{a}\right) \tag{35}$$

with fit parameters α, σ, C, and $\tilde{\alpha}$, cf. e.g. [17, 18].
The correction term

$$\Delta V_{\mathrm{lat}}(r) = \tilde{\alpha}\left(\frac{1}{r} - \frac{4\pi G(\mathbf{r}/a)}{a}\right) \tag{36}$$

is proportional to the difference between the continuum and lattice one gluon exchange expressions, cf. Sec. 2.2, which corresponds to the discretization errors of the lattice potential at tree-level of perturbation theory. Accordingly, the improved potential $V_{\mathrm{impr}}(r)$ is defined via the subtraction of the unphysical terms $\Delta V_{\mathrm{lat}}(r)$ and C describing lattice artifacts,

$$V_{\mathrm{impr}}(r) = V(r) - C - \Delta V_{\mathrm{lat}}(r)\ . \tag{37}$$

For this purpose, the values of $\Delta V_{\mathrm{lat}}(r)$ and C are determined by a four-parameter χ^2-minimizing fit of the unimproved lattice potential $V(r)$ to the parametrization given in Eq. (35).

Notably, for $\tilde{\alpha} = \alpha$ this definition is conceptually equivalent to the corrected r-improved potential proposed in Sec. 4.3, since in this case Eq. (35) can be written as

$$V(r)|_{\tilde{\alpha}=\alpha} = -\alpha \cdot \frac{4\pi G(\mathbf{r}/a)}{a} + \sigma r + C = -\alpha \cdot \frac{1}{r_{\mathrm{impr}}(\mathbf{r})} + \sigma r + C\ , \tag{38}$$

with r_{impr} defined as in Eq. (29). This expression is evidently very similar to Eq. (34). However, a noteworthy difference is that the values of the separation are not altered in the context of V-improvement, i.e. the resulting tree-level improved observable

$$V_{\mathrm{impr}}(r) = -\frac{\alpha}{r} + \sigma r \tag{39}$$

is a function of the original separation r.

The inclusion of an additional fit parameter $\tilde{\alpha}$ that can be adjusted separately from α is motivated by the next-to-leading order of perturbation theory, in which a shift of the coupling parameter from the so-called bare coupling to an effective coupling occurs (cf. [12] and references therein). While $V(r)|_{\tilde{\alpha}=\alpha}$ is an appropriate parametrization to define an improved potential based purely on tree-level perturbation theory as shown above, the additional degree of freedom in the fit helps to account for further deviations of the lattice data from this lowest-order approximation. Therefore, including $\tilde{\alpha}$ as a separate parameter is expected to provide a more comprehensive description of the discretization errors at small separations.

The expression for the V-improved potential given in Eq. (39) also holds for the general case $\tilde{\alpha} \neq \alpha$. Since this equation appears deceivingly similar to the fit function of the unimproved potential, cf. Eqs. (13) and (28), it should be reiterated that here, the values of the potential have been altered and the parameter α is determined via the four-parameter fit defined in Eq. (35), not simply by a fit of the unimproved data points to the standard Cornell parametrization.

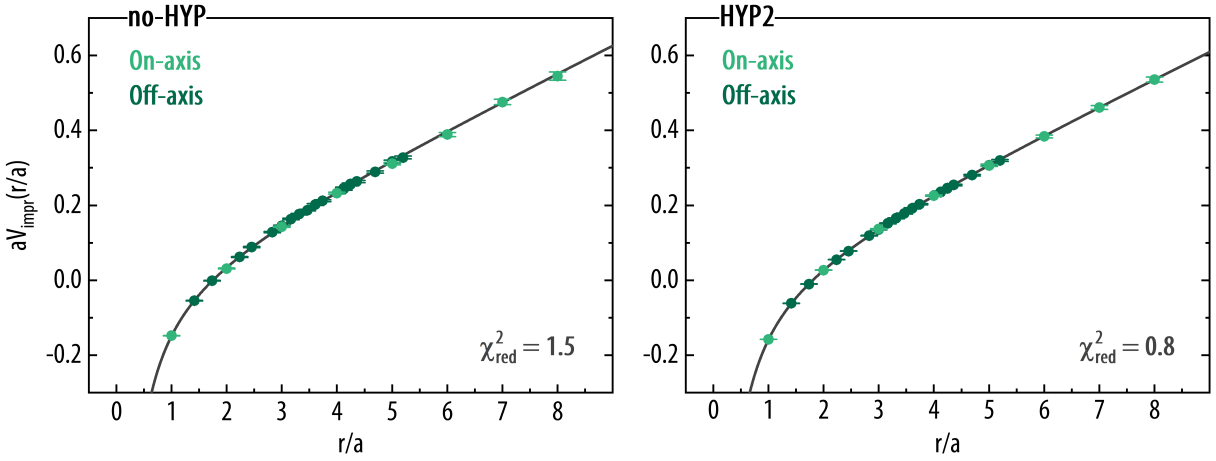

Figure 8: *The static potential after four-parameter fit improvement for the* no-HYP *and* HYP2 *discretizations. The improved potential and fit functions were computed using the fit parameters listed in Table 4.*

In Fig. 8, which shows the results of V-improvement for the *no-HYP* and *HYP2* lattice computations of the static potential, the highly successful restoration of rotational symmetry achieved by this method is immediately apparent. The data points of both computations are each very consistent across all on- and off-axis separations, which is reflected in the good fit convergence: the values of $\chi^2_{\text{red}} = 1.5$ and $\chi^2_{\text{red}} = 0.8$ for the fits of the *no-HYP* and *HYP2* potential, respectively, are close to ideal. For the *HYP2* potential in particular, this represents a considerable improvement compared to the previously discussed fits, which consistently returned values of $\chi^2_{\text{red}} > 10$ for this discretization.
Further, at both of the separations $r/a = 3$ and $r/a = 5$ mentioned in Sec. 4.1, there is no longer a difference between the on- and off-axis results for the potential at the same separation within statistical errors. These examples, which were not discussed for the r-improved potential due to the difference between the on- and off-axis values of r_{impr} preventing a direct comparison, provide another clearly visible indication of the restoration of rotational invariance.

	$\boldsymbol{\alpha}$	$\boldsymbol{a^2\sigma}$	$\boldsymbol{aC}$	$\boldsymbol{\tilde{\alpha}}$
no-HYP	0.220 ± 0.024	0.072 ± 0.004	0.540 ± 0.020	0.23 ± 0.09
HYP2	0.229 ± 0.010	0.0705 ± 0.0010	0.102 ± 0.007	0.259 ± 0.010

Table 4: *Fit parameters of the χ^2-minimizing fits of the static potential to the defining parametrization of four-parameter tree-level improvement. The fit ranges include all separations $1 \leq r/a \leq 8$.*

The results for the fit parameters of the V-improvement method's characteristic parametrization, cf. Eq. (35), are presented in Table 4 in lattice units. A comparison between the *no-HYP*

and *HYP2* values shows that the fit parameters α and $a^2\sigma$ are each in good agreement, with both values matching between discretizations within their respective error ranges. Further, the statistical errors are consistently smaller than those calculated for the r-improved potential for both the *no-HYP* and *HYP2* computations and all three parameters α, $a^2\sigma$, and aC shared by the fits used for these methods. It should be noted that similarly to the constants aC, the coefficient $\tilde{\alpha}$ is characterized by lattice artifacts and therefore not necessarily expected to match between different discretizations.

Furthermore, while the coefficients α and $\tilde{\alpha}$ are deliberately both included and therefore not required to be identical even within one discretization, they do match here for the *no-HYP* computation within statistical precision, cf. Table 4. This suggests that for this specific computation, the V-improvement of the potential is equivalent in concept to the r-improvement with the linear correction, as discussed above. Interestingly, it also appears to be similar in effect, since the value of $\chi^2_{\text{red}} = 1.5$ shared by the fits of both of these computations, cf. Figs. 6 and 8, indicates a similar degree of restoration of rotational invariance.
Conversely, the larger difference between the values of α and $\tilde{\alpha}$ for the *HYP2* discretization suggests a more significant contribution of higher-order perturbative correction terms to the parametrization of discretization errors at small separations, in accordance with the well-known short distance distortions of the potential occurring for this static action.

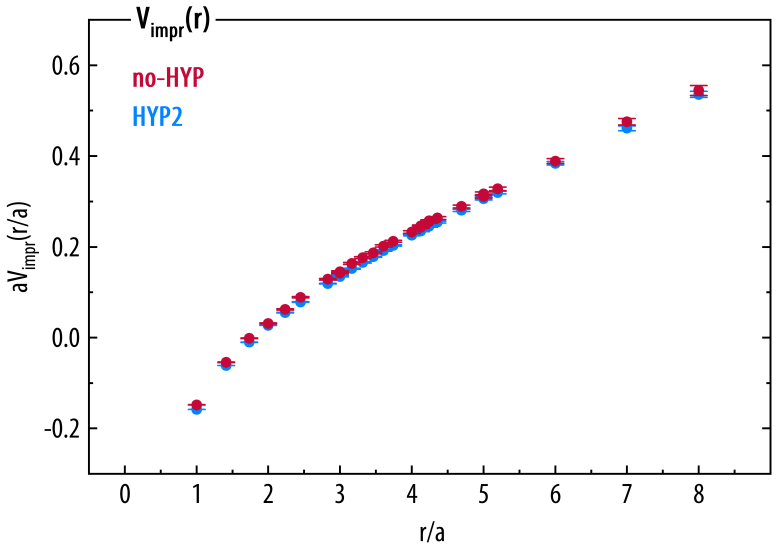

Figure 9: *Comparison between the* no-HYP *and* HYP2 *computations of the static potential with four-parameter tree-level improvement.*

Fig. 9 shows the direct comparison between the V-improved static potential in the *no-HYP* and *HYP2* discretizations. Since the constant aC of each computation is already subtracted in the definition of the improved potential, cf. Eq. (37), it is not necessary to account for this difference between discretizations in an additional step as described for the previous comparison graphs. Consequently, the values aC subtracted from the potential here were obtained by a fit including all separations, in contrast to the restricted fit ranges used to compute the values $(aC)'$ discussed above. Due to the resulting slightly lower precision of the subtracted constants, the data points of the *no-HYP* and *HYP2* computations shown in Fig. 9 appear to have a slight vertical shift relative to each other.

However, since the constant shift aC between discretizations is an unphysical lattice artifact to begin with, this does not affect the physically relevant aspect of Fig. 9, which is the excellent

agreement between the *no-HYP* and *HYP2* curves achieved by this method of tree-level improvement. While the corrected r-improved potential already shows good agreement between discretizations, cf. Fig. 7, slight deviations are discernible at very small separations $r/a \lesssim 2$. For the V-improved potential, even the data points at the lowest separations are remarkably consistent with a single curve, both in the comparison between different discretizations and between on- and off-axis Wilson loops, as shown in Fig. 8 and evidenced by the substantially improved fit convergences.

4.5 Sample application: setting the scale with the improved potential

As mentioned in the introduction, one of the reasons for the interest in precise computations of the static potential in lattice gauge theory is the important application of determining the lattice spacing a in physical units using the Sommer scale [7].

Since the calculation in the *HYP2* discretization in combination with V-improvement appears to be the least affected by both statistical and discretization errors as discussed in detail above, the lattice spacing of the computations performed in this work was determined using these values of the static potential.
Further, the Sommer parameter was set to the commonly used choice $r_0 = 0.5\,\mathrm{fm}$, resulting in

$$a = r_0 \sqrt{\frac{(a^2\sigma)'}{1.65 + \alpha'}} = (0.09679 \pm 0.00007)\,\mathrm{fm}\ . \tag{40}$$

The statistical error cited here was determined analogously to the fit parameters via a Jackknife analysis, with each Jackknife sample being defined by omitting one value of the potential. The Coulomb coefficient $\alpha' = 0.223 \pm 0.005$ and the string tension coefficient in lattice units $(a^2\sigma)' = 0.07018 \pm 0.00026$ were both obtained by a fit to the *HYP2* V-improved potential with a restricted fit range, as indicated by the prime, of $3 \leq r/a \leq 7$. This fit range is chosen to only include separations in sufficiently close proximity to the value of the Sommer parameter itself, in order to obtain an accurate result for the lattice spacing. Further details on this method of scale setting are discussed in Ref. [7].

5 Conclusion and outlook

For lattice gauge theory computations of the static potential, the four-parameter fit method of tree-level improvement appears to be more effective at reducing discretization errors than the method of improved separation, which shows clear signs of remaining lattice artifacts and even an overcorrection of the values of the potential.
This claim is substantiated not only by the extensive comparisons presented above, which include the computation of numerous on- and off-axis Wilson loops using two different static actions, but also in particular by the discussion of the corrected r-improved potential. Here, the subtraction of the proposed correction term evidently results in a significantly better restoration of rotational symmetry and agreement between discretizations, therefore providing a convincing and self-consistent explanation for the problems seen with the method of improved separation.

In terms of practicality, the method of improved separation is the easiest to implement, since it essentially only involves determining the values of the lattice propagator and then replacing the separation with the improved separation accordingly. The four-parameter fit improvement method requires an additional χ^2-minimizing fit as indicated by the name, as well as a final step of adjusting the values of the potential according to the resulting fit parameters.
Using the method of improved separation and then correcting the results returns considerably more accurate results than the method of improved separation alone. However, this is certainly the most impractical approach, since it involves first calculating the improved separation, then determining the string breaking coefficient – e.g., by a χ^2-minimizing fit of the potential with an appropriate fit range – and lastly subtracting the correction term from the values of the potential. Therefore, this approach not only still returns slightly worse results than four-parameter fit improvement, likely due to the inclusion of the additional parameter $\tilde{\alpha}$ in the latter method, but it also negates the main advantage of the method of improved separation, which is the easy implementation without the reliance on a fit.

Ultimately, the concern about an effective improvement of the static potential likely outweighs the minor differences in practicality between the methods. In this case, the results discussed in this thesis strongly suggest the four-parameter fit improvement as the method of choice.

These results, which were obtained in this work using simulations in SU(2) lattice gauge theory, further motivate interesting directions for future research. Exploring the discussed methods of tree-level improvement in SU(3) lattice gauge theory, or even in full lattice QCD with dynamical fermions, could be a step towards numerical simulations approximating the physical reality of a quark-antiquark pair in nature more closely, at the cost of considerably more computationally demanding simulations. Further, incorporating a set of multiple different discretizations, such as varying lattice spacings, in addition to the computations considered in this thesis could allow quantitative insight into the influence of the lattice spacing on discretization errors, as well as provide additional comparisons between methods of tree-level improvement.

Acknowledgements

First, I would like to thank my supervisors Marc Wagner and Carolin Schlosser for their excellent guidance and support. I highly appreciate the time they took to always answer any questions I had, the invaluable advice not only on the subject matter of this thesis but on the technical implementation, scientific research and writing, as well as my studies as a whole. I thank them for the many long, helpful discussions, without which this thesis would not have been possible, and for the opportunity to study this exciting field, which allowed me to gain many new insights about QCD, programming, and modern research in theoretical physics.

I also want to thank my friends and family for always supporting me through my studies. Specifically, I am grateful to Lara Denninger for her helpful advice on formatting and graphing, as well as to everyone who helped me proof-read this thesis. I appreciate the time and effort and thank them for their advice and support.

References

[1] C. N. Yang and R. L. Mills, "Conservation of Isotopic Spin and Isotopic Gauge Invariance," Phys. Rev. **96**, 191 (1954).

[2] M. E. Peskin and D. V. Schroeder, "An Introduction to Quantum Field Theory" (1st ed.), Addison-Wesley, Reading (1995).

[3] O. Philipsen, "Quantenfeldtheorie und das Standardmodell der Teilchenphysik: Eine Einführung" (1st ed.), Springer Spektrum, Berlin/Heidelberg (2018).

[4] K. G. Wilson, "Confinement of quarks," Phys. Rev. D **10**, 2445 (1974).

[5] J. B. Kogut, R. B. Pearson, and J. Shigemitsu, "Quantum-Chromodynamic β Function at Intermediate and Strong Coupling," Phys. Rev. Lett. **43**, 484 (1979).

[6] M. Creutz, "Monte Carlo study of quantized SU(2) gauge theory," Phys. Rev. D **21**, 2308 (1980).

[7] R. Sommer, "A New Way to Set the Energy Scale in Lattice Gauge Theories and its Application to the Static Force and α_s in SU(2) Yang-Mills Theory," Nucl. Phys. B **411**, 839 (1994) [arXiv:hep-lat/9310022v1].

[8] A. Bazavov, N. Brambilla, X. Garcia i Tormo, P. Petreczky, J. Soto, and A. Vairo, "Determination of α_s from the QCD static energy: an update," Phys. Rev. D **90**, 074038 (2014) [arXiv:1407.8437v3 [hep-ph]].

[9] A. Bazavov, N. Brambilla, X. Garcia i Tormo, P. Petreczky, J. Soto, A. Vairo, and J. H. Weber, "Determination of the QCD coupling from the static energy and the free energy," Phys. Rev. D **100**, 114511 (2019) [arXiv:1907.11747v1 [hep-lat]].

[10] C. B. Lang and C. Rebbi, "Potential and restoration of rotational symmetry in SU(2) lattice gauge theory," Phys. Lett. B **115**, 137 (1982).

[11] R. Sommer and K. Schilling, "Testing the Rotational Symmetry of the SU(3) Potential," Z. Phys. C **29**, 95 (1985).

[12] C. Michael, "The Running Coupling from Lattice Gauge Theory," Phys. Lett. B **283**, 103 (1992) [arXiv:hep-lat/9205010v1].

[13] S. P. Booth, A. Hulsebos, A. C. Irving, A. McKerrell, C. Michael, P. S. Spencer, and P. W. Stephenson (UKQCD Collaboration), "SU(2) Potentials from Large Lattices," Nucl. Phys. B **394**, 509 (1993) [arXiv:hep-lat/9209007v1].

[14] G. S. Bali and K. Schilling, "Running Coupling and the Λ-Parameter from SU(3) Lattice Simulations," Phys. Rev. D **47**, 661 (1993) [arXiv:hep-lat/9208028v1].

[15] H. Wittig (UKQCD Collaboration), "New Results From UKQCD Using the Cray T3D: Measuring Gluonic Observables," Nucl. Phys. Proc. Suppl. **42**, 288 (1995) [arXiv:hep-lat/9411075v1].

[16] R. G. Edwards, U. M. Heller, and T. R. Klassen, "Accurate Scale Determinations for the Wilson Gauge Action," Nucl. Phys. B **517**, 377 (1998) [arXiv:hep-lat/9711003v2].

[17] A. Hasenfratz, R. Hoffmann, and F. Knechtli, "The Static Potential with Hypercubic Blocking," Nucl. Phys. Proc. Suppl. **106**, 418 (2002) [arXiv:hep-lat/0110168v1].

[18] C. Schlosser and M. Wagner, "Hybrid static potentials in SU(3) lattice gauge theory at small quark-antiquark separations," Phys. Rev. D **105**, 054503 (2022) [arXiv:2111.00741v1 [hep-lat]].

[19] M. Guagnelli, R. Sommer, and H. Wittig, "Precision computation of a low-energy reference scale in quenched lattice QCD," Nucl. Phys. B **535**, 389 (1998) [arXiv:hep-lat/9806005v2].

[20] S. Necco and R. Sommer, "The $N_f = 0$ heavy quark potential from short to intermediate distances," Nucl. Phys. B **622**, 328 (2002) [arXiv:hep-lat/0108008v1].

[21] M. Donnellan, F. Knechtli, B. Leder, and R. Sommer (ALPHA Collaboration), "Determination of the Static Potential with Dynamical Fermions," Nucl. Phys. B **849**, 45 (2011) [arXiv:1012.3037v3 [hep-lat]].

[22] N. Brambilla, V. Leino, O. Philipsen, C. Reisinger, A. Vairo, and M. Wagner, "Lattice gauge theory computation of the static force," Phys. Rev. D **105**, 054514 (2022) [arXiv:2106.01794v2 [hep-lat]].

[23] G. S. Bali and A. Pineda, "QCD phenomenology of static sources and gluonic excitations at short distances," Phys. Rev. D **69**, 094001 (2004) [arXiv:hep-ph/0310130v1].

[24] K. Jansen, F. Karbstein, A. Nagy, and M. Wagner (ETM Collaboration), "$\Lambda_{\overline{\text{MS}}}$ from the static potential for QCD with $n_f = 2$ dynamical quark flavors," JHEP **1201**, 025 (2012) [arXiv:1110.6859v3 [hep-ph]].

[25] A. Bazavov, N. Brambilla, P. Petreczky, A. Vairo, and J. H. Weber (TUMQCD collaboration), "Color screening in (2+1)-flavor QCD," Phys. Rev. D **98**, 054511 (2018) [arXiv:1804.10600v2 [hep-lat]].

[26] F. Karbstein, M. Wagner, and M. Weber, "Determination of $\Lambda_{\overline{\text{MS}}}^{(n_f=2)}$ and analytic parameterization of the static quark-antiquark potential," Phys. Rev. D **98**, 114506 (2018) [arXiv:1804.10909v3 [hep-ph]].

[27] C. Gattringer and C. B. Lang, "Quantum Chromodynamics on the Lattice: An Introductory Presentation" (1st ed.), Lect. Notes Phys. **788**, Springer, Berlin/Heidelberg (2010).

[28] H. J. Rothe, "Lattice Gauge Theories: An Introduction" (4th ed.), World Sci. Lect. Notes Phys. **82**, World Scientific Publishing Co. Pte. Ltd. (2012).

[29] C. Riehl and M. Wagner, "Hybrid static potentials in SU(2) lattice gauge theory at short quark-antiquark separations" (2020) [arXiv:2008.12216v1 [hep-lat]].

[30] P. Wolf and M. Wagner, "Lattice study of hybrid static potentials," J. Phys. Conf. Ser. **599**, 012005 (2015) [arXiv:1410.7578v3 [hep-lat]].

[31] L. Müller, O. Philipsen, C. Reisinger, and M. Wagner, "Hybrid static potential flux tubes from SU(2) and SU(3) lattice gauge theory," Phys. Rev. D **100**, 054503 (2019) [arXiv:1907.01482v2 [hep-lat]].

[32] K. Symanzik, "Some topics in quantum field theory," Lect. Notes Phys. **153**, Springer Berlin Heidelberg (1981).

[33] P. Weisz, "Continuum limit improved lattice action for pure Yang-Mills theory (I)," Nucl. Phys. B **212**, 1 (1983).

[34] S. Lottini, O. Philipsen, and M. Wagner, "Quantenfeldtheorie II," Lecture notes, Goethe-Universität Frankfurt am Main (2013).

[35] U. Heller and F. Karsch, "One-loop perturbative calculation of Wilson loops on finite lattices," Nucl. Phys. B **251**, 254 (1985).

[36] E. Eichten and B. Hill, "An effective field theory for the calculation of matrix elements involving heavy quarks," Phys. Lett. B **234**, 511 (1990).

[37] A. Hasenfratz and F. Knechtli, "Flavor Symmetry and the Static Potential with Hypercubic Blocking," Phys. Rev. D **64**, 034504 (2001) [arXiv:hep-lat/0103029v2].

[38] M. Della Morte, S. Durr, J. Heitger, H. Molke, J. Rolf, A. Shindler, and R. Sommer (ALPHA Collaboration), "Lattice HQET with exponentially improved statistical precision," Phys. Lett. B **581**, 93 (2004) [Erratum: Phys. Lett. B **612**, 313 (2005)], [arXiv:hep-lat/0307021v3].

[39] M. Della Morte, A. Shindler, and R. Sommer (ALPHA Collaboration), "On lattice actions for static quarks," JHEP **0508**, 051 (2005) [arXiv:hep-lat/0506008v1].

[40] M. Lüscher and P. Weisz, "Coordinate space methods for the evaluation of Feynman diagrams in lattice field theories," Nucl. Phys. B **445**, 429 (1995) [arXiv:hep-lat/9502017v2].

[41] A. Grimbach, D. Guazzini, F. Knechtli, and F. Palombi (ALPHA Collaboration), "O(a) improvement of the HYP static axial and vector currents at one-loop order of perturbation theory," JHEP **0803**, 039 (2008) [arXiv:0802.0862v1 [hep-lat]].

[42] M. Albanese *et al.* (APE Collaboration), "Glueball masses and string tension in lattice QCD," Phys. Lett. B **192**, 163 (1987).

[43] S. Capitani, O. Philipsen, C. Reisinger, C. Riehl, and M. Wagner, "Precision computation of hybrid static potentials in SU(3) lattice gauge theory," Phys. Rev. D **99**, 034502 (2019) [arXiv:1811.11046v3 [hep-lat]].

[44] K. Jansen, C. Michael, A. Shindler, and M. Wagner (ETM Collaboration), "The static-light meson spectrum from twisted mass lattice QCD," JHEP **0812**, 058 (2008) [arXiv:0810.1843v1 [hep-lat]].

[45] G. S. Bali, H. Neff, T. Düssel, T. Lippert, and K. Schilling (SESAM Collaboration), "Observation of String Breaking in QCD," Phys. Rev. D **71**, 114513 (2005) [arXiv:hep-lat/0505012v2].

[46] J. Shao and D. Tu, "The Jackknife and Bootstrap" (1st ed.), Springer Series in Statistics, Springer, New York (1996).

[47] M. Wagner, "Numerical methods in physics," Lecture notes, Goethe-Universität Frankfurt am Main (2021).

[48] W. H. Press, S. A. Teukolsky, W. T. Vetterling, and B. P. Flannery, "Numerical Recipes in C++: The Art of Scientific Computing" (2nd ed.), Cambridge University Press, New York (2002).

[49] R. Sommer, "Scale setting in lattice QCD," PoS LATTICE **2013**, 015 (2013) [arXiv:1401.3270v1 [hep-lat]].

Erklärung nach § 30 (12) Ordnung für den Bachelor- und den Masterstudiengang

Hiermit erkläre ich, dass ich die Arbeit selbstständig und ohne Benutzung anderer als der angegebenen Quellen und Hilfsmittel verfasst habe. Alle Stellen der Arbeit, die wörtlich oder sinngemäß aus Veröffentlichungen oder aus anderen fremden Texten entnommen wurden, sind von mir als solche kenntlich gemacht worden. Ferner erkläre ich, dass die Arbeit nicht – auch nicht auszugsweise – für eine andere Prüfung verwendet wurde.

Frankfurt, den 04.07.2022

_____

Sonja Köhler